

AKÜ FEMÜBİD 16 (2016) 025201(276-284)
DOI: 10.5578/fmbd.27642

AKU J. Sci. Eng. 16 (2016) 025201(276-284)

Araştırma Makalesi / Research Article

Farklı Dielektrik Ortamların İçerisindeki Dielektrik Küreden Saçılan Alanların Analizi: Kaynak ve Gözlem Noktalarının Karşılıklı Olması Durumunda

Emine AVŞAR AYDIN¹, Nezahat GÜNENÇ TUNCEL²

¹ Çukurova Üniversitesi, Mühendislik-Mimarlık Fakültesi, Elektrik-Elektronik Mühendisliği Bölümü, Adana.
e-mail:avsare@cu.edu.tr, rasvaenime@gmail.com

²Osmaniye Korkut Ata Üniversitesi, Mühendislik-Mimarlık Fakültesi, Elektrik-Elektronik Mühendisliği Bölümü, Osmaniye. E-mail:nezahattuncel@osmaniye.edu.tr

Geliş Tarihi: 14.01.2016; Kabul Tarihi: 29.08.2016

Özet

Kanonik yapılardan elektromanyetik saçılma, elektromanyetik teoride önemli bir konudur. Bu çalışmada, dielektrik geçirgenliği frekansa bağlı olan bir dielektrik küreden elektromanyetik saçılma problemi, gelen dalganın eğik gelmesi durumu için çözülmüştür. Bu çalışmada küre, bir tümörün elektromanyetik modeli olarak düşünüldüğü için frekansa bağlılık Cole-Cole model ile gösterilmiştir. Cole-Cole model, biyolojik dokuların elektromanyetik olarak modellenmesi literatürde sıkça kullanılan bir modeldir. Gelen dalga H-polarize olarak düzlem dalga olarak varsayılmıştır. Küre yüzeyinden saçılan alan ve küre içerisine iletilen alan ifadeleri Helmholtz denkleminde faydalanılarak bilinmeyen katsayılı fonksiyonlar şeklinde yazılmıştır. Daha sonra, bu bilinmeyen katsayılar sınır koşulları aracılığıyla belirlenmiştir. Elde edilen saçılan ve iletilen alan ifadesi, bistatik hal için nümerik olarak incelenmiştir. Elde edilen saçılan alanın ifadesinin doğrulanması için kürenin elektromanyetik özellikleri dielektrik küreye indirgenmiş ve saçılan alanın ifadeleri Harrington'un kitabındaki sonuçlar ile karşılaştırılmıştır. Sonuçlar, alıcı ve verici kaynaklarının karşılıklı dönmesiyle daha hızlı ve daha iyi elde edilmiştir. Ultra-geniş bant radar-tabanlı görüntüleme yaklaşımı, kötü huylu meme tümörleri gibi önemli saçılım engellerinin sadece varlığını ve yerini belirlemesine odaklanan daha basit hesaplamalı bir problemi daha hızlı çözebilmektedir. Bundan dolayı, bu yöntem biyomedikal mühendisliğinde alternatif tarama ve teşhis aracı olarak kullanılabilir.

Anahtar kelimeler

Saçılım, Dielektrik küre,
Kanonik yapı, Eğik
gelme, Karşılıklı
dönme.

Analysis of the Scattering Fields by Dielectric Sphere inside Different Dielectric Mediums: The Case of the Source and Observation Point is Reciprocal

Abstract

The electromagnetic scattering from canonical structure is an important issue in electromagnetic theory. In this study, the electromagnetic scattering from dielectric sphere with oblique incidence is investigated. While an incident wave comes with a certain angle, observation point turns from 0 to 360 degrees. The electromagnetic field is considered as a plane wave with H polarized. The scattered and transmitted field expressions with unknown coefficients are written. The unknown coefficients are obtained by using exact boundary conditions. Then, the sphere is considered as having frequency dependent dielectric permittivity. The frequency dependence is shown by Cole-Cole model. The analytic results are compared with scattered field by dielectric sphere obtained by Harrington. The results are obtained faster and more reliable with reciprocal rotation. Ultra-wide band (UWB) radar-based imaging approach can solve a simpler computational problem faster dealing with only to identify the presence and location of significant scattering obstacles such malignant breast tumours. Therefore, it can be used in biomedical engineering as an alternative screening and diagnosis tool.

Keywords

Scattering, Dielectric
sphere, Canonical
structure, Oblique
incidence, reciprocal
rotation.

1. Introduction

The electromagnetic scattering by a sphere has a high application potential in electromagnetics. Lord Rayleigh (1871) studied light diffraction from a small particle of spherical shape. The sphere is considered as very small according to the wavelength and also the difference of dielectric constant of sphere and surrounding medium is small. Love (1899) investigated the plane wave scattering by a dielectric sphere with any size and any dielectric constant. Weston and Hemenger (1962) calculate the backscattering by conducting sphere coated with large complex refraction index material by reducing the problem to general impedance boundary problem. Swarner and Peters (1963) calculated RCS of sphere and cylinders with homogenous dielectric and plasma coating. Calculations are done by using both exact boundary value solutions and semi-empirical approximate solution and results are compared. Good agreement is obtain between two methods while radii of obstacles are in Rayleigh region. Rheinstein (1963) investigated scattering problem from dielectric coated conducting sphere with different thickness of coating and indicate that RCS of dielectric coated conductor sphere greater than the conductor sphere because of interference effects. Diffracted and backscattering field is obtained by using geometric optics for small wavelengths. Scattering field by a large dense dielectric sphere is obtained by using GO approximation and Mie series by Inada and Plonus (1970). Richmond (1987) investigated the electromagnetic scattering by lossy, homogeneous and isotropic ferrite coating conducting sphere. The eigenfunctions formulation, PO and GO approximations is used for solution and numerical results and bistatic scattering patterns are presented. Also, this study shows that contribution of Mie series (surface waves) is larger than GO approximation. Hill (1988) shows that Born approximation can be used to calculate scattered

field by dielectric sphere. Hamid et. al. (1991) investigated scattering by a dielectric sphere with concentric sphere shell. The RCS of the system is also presented. Scattering by an impedance sphere coated with uniaxial anisotropic layer is investigated by (Geng et. al. 2009). Obtained general solution is also reduced to the some isotropic subcases and results are presented.

In this study, the scattered field expressions from a dielectric sphere are obtained. The difference between the incidence and observation point is 180°. The numerical results are presented for incidence angle from 0° to 360°. The scattered field is calculated for sphere radius 3mm and 8mm. Also, the scattered field are shown in graphics for various frequency to show the frequency dependence explicitly.

2. Analytical Study

Electromagnetic waves have a huge application area, especially in biomedical engineering. There are many passive and active microwave techniques for early detection of breast cancer.

There is a significant contrast in the electrical properties of the normal and the malignant breast tissues. In order to obtain the information about the existence and position of the malignant tumour, it is important to understand the electromagnetic scattering behavior of the tumour. Therefore, cylindrically and spherically shaped tumour models have been studied to estimate the electromagnetic scattering features.

The frequency dependence of dielectric properties of the breast fat, tumour, and fibroglandular tissues are frequently modelled by using the single pole Cole-Cole model:

$$\varepsilon = \varepsilon_{\infty} + \frac{(\varepsilon_s - \varepsilon_{\infty})}{1 + (j\omega\tau)^{1-\alpha}} - j \frac{\sigma_s}{\omega\varepsilon_0} \quad (29)$$

where ε_s is the relative low-frequency permittivity, ε_{∞} is the relative high-frequency permittivity, τ is the relaxation time, ε_0 is the permittivity of free-space, and ω is the angular frequency and σ_s is the ionic conductivity.

In addition, the Debye model permits very fast computation, but it is not adequate to describe the tissue dispersion in the whole frequency spectrum. On the contrary the Cole-Cole model is considered the most reliable fitting tool to describe tissue dielectric properties. Because of this, Cole-Cole model is preferred.

The electromagnetic scattering by a sphere is investigated for the bistatic case. The incident wave is assumed as a plane wave and propagates along the z and y direction. For the frequency dependence of the sphere Cole-Cole model is used. The geometry of the problem is shown in Fig. 1.

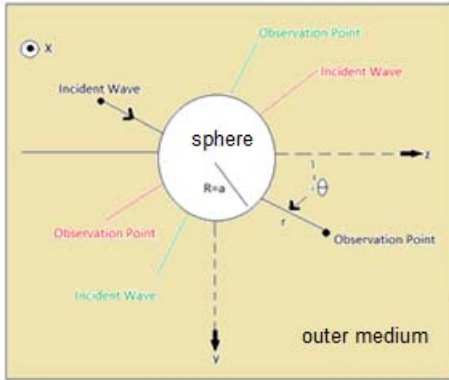


Figure 1. Illustration of method in this study

$$\vec{E}^i = E_0 e^{-jkz} \vec{a}_x \quad (1)$$

$$\vec{H}^i = H_0 e^{-jkz} \vec{a}_y \quad (2)$$

The scattered field will be generated by an A_r and F_r of the same form as the incident field with \hat{J}_n replaced by $\hat{H}_n^{(2)}$. Hence, we construct scattered potentials as Harrington (1961):

$$\begin{aligned} A_r^+ &= \frac{E_0}{\omega\mu} \cos(\theta) \\ &\times \sum_{n=1}^{\infty} [a_n \hat{J}_n(kr) + b_n \hat{H}_n^{(2)}(kr)] P_n^1(\cos(\theta)) \end{aligned} \quad (3)$$

$$\begin{aligned} F_r^+ &= \frac{E_0}{k} \sin(\theta) \\ &\times \sum_{n=1}^{\infty} [a_n \hat{J}_n(kr) + c_n \hat{H}_n^{(2)}(kr)] P_n^1(\cos(\theta)) \end{aligned} \quad (4)$$

for outside the spherical tumour ($r > a$), and

$$\begin{aligned} A_r^- &= \frac{E_0}{\omega\mu} \cos(\theta) \\ &\times \sum_{n=1}^{\infty} d_n \hat{J}_n(k_a r) P_n^1(\cos(\theta)) \end{aligned} \quad (5)$$

$$\begin{aligned} F_r^- &= \frac{E_0}{k} \sin(\theta) \\ &\times \sum_{n=1}^{\infty} e_n \hat{J}_n(k_a r) P_n^1(\cos(\theta)) \end{aligned} \quad (6)$$

for inside the spherical tumour ($r < a$),

where $\hat{J}_n(kr) = kr j_n(kr)$, $\hat{H}_n^{(2)}(kr) = kr h_n^{(2)}(kr)$, Expression for the Legendre polynomials is given by Rodrigues' formula

$$P_n(u) = \frac{1}{2^n n!} \frac{d^n}{du^n} (u^2 - 1)^n, \quad u = \cos(\theta) \quad (7)$$

Solution to the associated Legendre equation is

$$P_n^m(u) = (-1)^m (1 - u^2)^{m/2} \frac{d^m P_n(u)}{du^m} \quad (8)$$

$$\begin{aligned} P_n^1(u) &= P_n^1(\cos(\theta)) \\ &= \frac{\partial P_n(\cos(\theta))}{\partial \theta} \end{aligned} \quad (9)$$

$$P_n^1(u) = \frac{1}{1-u^2} [-nuP_n^1(u) + (n+m)P_{n-1}^1(u)] \quad (10)$$

$$a_n = \frac{j^{-n}(2n+1)}{n(n+1)} \quad (11)$$

$$k = \frac{\sqrt{\omega^2 \varepsilon \varepsilon_0 \mu - j\sigma \omega \mu}}{\sqrt{\omega^2 \varepsilon_d \varepsilon_0 \mu_d - j\sigma_d \omega \mu_d}}, \quad k_d = \quad (12)$$

$j_n, y_n,$ and $h_n^{(2)}$ are the spherical Bessel functions of the first order, Bessel functions of the second order and Hankel functions of the second kind, respectively. J_n and Y_n are regular Bessel function of the first order and second order, respectively. These functions can be written as Korenev (2002):

$$\begin{aligned} j_n(x) &= \sqrt{\frac{\pi}{2x}} J_{n+\frac{1}{2}}(x), \\ y_n(x) &= \sqrt{\frac{\pi}{2x}} Y_{n+\frac{1}{2}}(x), \\ h_n^{(2)} &= j_n(x) - iy_n(x). \end{aligned} \quad (13)$$

To work with these expressions numerically and from a simulation point of view, it is convenient to introduce the Riccati-Bessel functions and the Riccati-Hankel functions. Riccati-Bessel functions only slightly differ from spherical Bessel functions Malicky and Malicka (1990):

$$\begin{aligned} \psi_n(x) &= xj_n(x) = \sqrt{\frac{\pi x}{2}} J_{n+\frac{1}{2}}(x), \\ C_n(x) &= -xy_n(x) = -\sqrt{\frac{\pi x}{2}} Y_{n+\frac{1}{2}}(x), \\ \varsigma_n(x) &= xh_n^{(2)}(x) = \sqrt{\frac{\pi x}{2}} H_{n+\frac{1}{2}}(x) \\ &= \psi_n(x) + iC_n(x). \end{aligned} \quad (14)$$

It is useful to simplify, by using the Riccati-Bessel functions. It is found that Margerum and Vand (1964):

$$\begin{aligned} [\psi_n(x)]^l &= [xj_n(x)]^l = \hat{f}_n^l(x) \\ &= j_n(x) + xj_n^l(x) \end{aligned} \quad (15)$$

Recalling the recursion relations for the derivatives we have

$$xj_n^l(x) = xj_{n-1}(x) - (n+1)j_n(x) \quad (16)$$

We thus find that:

$$\begin{aligned} \psi_n^l(x) &= \hat{f}_n^l(x) = j_{n-1}(x) - nj_n(x) \\ &= \psi_{n-1}(x) - \frac{n}{x}\psi_n(x) \\ C_n^l(x) &= C_{n-1}(x) - \frac{n}{x}C_n(x) \end{aligned}$$

$$\begin{aligned} \varsigma_n^l(x) &= \hat{H}_n^{(2)l}(x) = h_{n-1}^{(2)}(x) - nh_n^{(2)}(x) \\ &= \varsigma_{n-1}(x) - \frac{n}{x}\varsigma_n(x) \end{aligned} \quad (17)$$

or

$$\begin{aligned} \varsigma_n^l(x) &= \hat{H}_n^{(2)l}(x) = \psi_n^l(x) + iC_n^l(x) \end{aligned}$$

With the continuity of $E_\theta^+ = E_\theta^-, E_\theta^+ = E_\theta^-, H_\theta^+ = H_\theta^-,$ and $H_\theta^+ = H_\theta^-$ at $r=a,$ one can obtain the closed form equations of the unknown constants; b_n, c_n, d_n and $e_n,$ as follows:

$$\begin{aligned} b_n &= a_n \frac{\xi \hat{J}_n^l(ka) \hat{J}_n(k_a a) - \xi_a \hat{J}_n(ka) \hat{J}_n^l(k_a)}{\xi_a \hat{H}_n^{(2)}(ka) \hat{J}_n^l(k_a a) - \xi \hat{H}_n^{(2)l}(ka) \hat{J}_n(k_a)} \end{aligned} \quad (18)$$

$$\begin{aligned} c_n &= a_n \frac{k\mu_a \hat{J}_n(k_a a) \hat{J}_n^l(ka) - k_a \mu \hat{J}_n^l(k_a a) \hat{J}_n(ka)}{k_a \mu \hat{J}_n^l(k_a a) \hat{H}_n^{(2)}(ka) - k\mu_a \hat{J}_n(k_a a) \hat{H}_n^{(2)l}(ka)} \end{aligned} \quad (19)$$

$$d_n = a_n \frac{\xi \hat{H}_n^{(2)l}(ka) \hat{J}_n(ka) - \xi \hat{H}_n^{(2)}(ka) \hat{J}_n^l(ka)}{\xi \hat{H}_n^{(2)l}(ka) \hat{J}_n(ka) - \xi_d \hat{H}_n^{(2)}(ka) \hat{J}_n^l(ka)} \quad (20)$$

$$e_n = a_n \frac{k \mu_d \hat{H}_n^{(2)l}(ka) \hat{J}_n(ka) - k_d \mu \hat{H}_n^{(2)}(ka) \hat{J}_n^l(ka)}{k \mu_d \hat{H}_n^{(2)l}(ka) \hat{J}_n(ka) - k_d \mu \hat{H}_n^{(2)}(ka) \hat{J}_n^l(ka)} \quad (21)$$

where $\xi = k/(\sigma + j\omega\epsilon\epsilon_0)$ and $\xi_d = k_d/(\sigma_d + j\omega\epsilon_d\epsilon_0)$.

The resulting scattering field components are follows:

$$E_{rs} = \frac{E_0 k \xi}{\omega \mu} \cos(\phi) \left[\sum_{n=1}^{\infty} b_n \hat{H}_n^{(2)}(kr) P_n^1(\cos(\theta)) + \frac{E_0 k \xi}{\omega \mu} \cos(\phi) \left[\sum_{n=1}^{\infty} b_n \hat{H}_n^{(2)u}(kr) P_n^1(\cos(\theta)) \right] \quad (22)$$

$$E_{\theta s} = -\frac{E_0}{kr} \cos(\phi) \frac{1}{\sin(\theta)} \left[\sum_{n=1}^{\infty} c_n \hat{H}_n^{(2)}(kr) P_n^1(\cos(\theta)) + \frac{-E_0 \xi}{r \omega \mu} \cos(\phi) \sin(\theta) \left[\sum_{n=1}^{\infty} b_n \hat{H}_n^{(2)l}(kr) P_n^1(\cos(\theta)) \right] \quad (23)$$

$$E_{\phi s} = \frac{-E_0 \sin(\theta) \sin(\phi)}{kr} \left[\sum_{n=1}^{\infty} c_n \hat{H}_n^{(2)}(kr) P_n^1(\cos(\theta)) + \frac{-E_0 \xi}{r \omega \mu \sin(\theta)} \sin(\phi) \left[\sum_{n=1}^{\infty} b_n \hat{H}_n^{(2)l}(kr) P_n^1(\cos(\theta)) \right] \quad (24)$$

For the verification of the results, the electromagnetic properties of the sphere is reduced to dielectric to compare with the scattered field expressions in [Harrington referans]. For the bistatic case, the coordinate transform is applied to

the scattered field. The coordinate transform is shown in Figure 2.

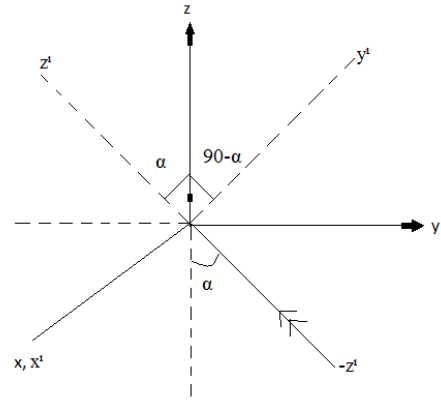


Figure 2. The coordinate illustration of the problem

$$z' = z \cdot \cos \alpha - y \cdot \sin \alpha \quad (25)$$

$$z' = r' \cos \theta' = r \cdot \cos(\theta - \alpha) \cdot \cos \alpha - r \cdot \sin(\theta - \alpha) \cdot \sin \alpha \quad (26)$$

$$r' \cos \theta' = r \cdot \{ \cos(\theta - \alpha) \cdot \cos \alpha - \sin(\theta - \alpha) \cdot \sin \alpha \}$$

$$r' = r \quad (27)$$

$$\cos \theta' = \cos(\theta - \alpha) \cdot \cos \alpha - \sin(\theta - \alpha) \cdot \sin \alpha$$

$\phi=90$ and so

$$\cos \theta' = \left(\frac{(1 + \sin \phi)}{2} * \cos \theta + \frac{(1 - \sin \phi)}{2} * \cos(\theta - 2\alpha) \right) \quad (28)$$

Then, the scattered field expression is obtained by substituting Eq. (28) into Eq. (22-24) for bistatic case.

3. Numerical Results and Discussions

The analytical results of the scattered fields (E_ϕ , E_θ) with respect observation angle for different incident angle and operation frequency are shown

in Fig.3-Fig.10. The magnetic permeability of both outer medium and dielectric sphere are taken as $4\pi \cdot 10^{-7}$ (H/m) and dielectric permittivity is given in Table 1. E_0 is 1 V/m and radial measurement distance is 30 mm.

Table 1. Single Pole Cole-Cole Parameters for Fat Tissues (Kim and Pack, 2012)

Tissue Type	ϵ_s	ϵ_∞	τ [ps]	α	σ (S/m)
Tumor	4	91.68	23.42	0.6106	0.8985
Fibro-glandular	2.5	76.31	35.10	0.6087	0.8825
Fat	2.5	8.74	99.73	0.2055	0.0879

When the scattered fields with respect to observation angle for different frequencies and different tumour diameters of both 6mm and 16mm are obtained, the scattered fields are distributed around the dielectric sphere for low frequencies. In addition, an incident electromagnetic wave impinges to sphere in the 1-8 GHz frequency range. The dielectric properties of the sphere is given in Table 1. The comparison of the magnitude of the ϕ and θ component of the scattered field for two different frequencies are shown in Fig. 3 and Fig. 5 for the sphere with 3 mm radii. It is easily seen from the graphics that the scattered field reaches the maximum value in the diffraction of the incident wave for both $E_{\phi s}$ and $E_{\theta s}$ as expected. In figure 4 and 6, the scattered field versus observation angle is presented for 8 mm dielectric sphere. The magnitude of the scattered field for 8 mm sphere is smaller than the sphere with 3 mm radii.

In this part, 4.5 GHz and 8 GHz are used, since the simulation is performed frequencies between 1 GHz and 8GHz in CST Microwave Studio. Also, sphere size is take into accounted.

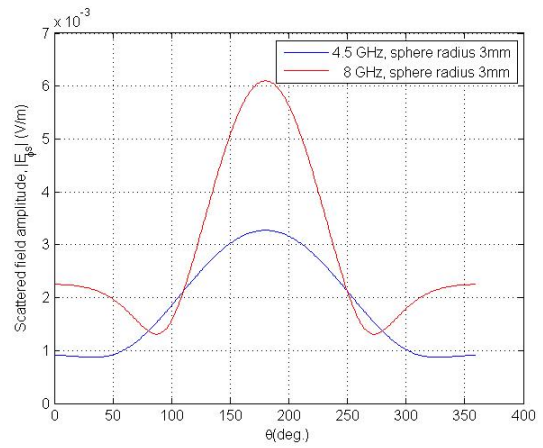


Figure 3. Comparison of scattered field, $|E_{\phi s}|$ with respect to observation angles, for different frequencies for a dielectric sphere radius of 3mm (incident angle is constant, 180°)

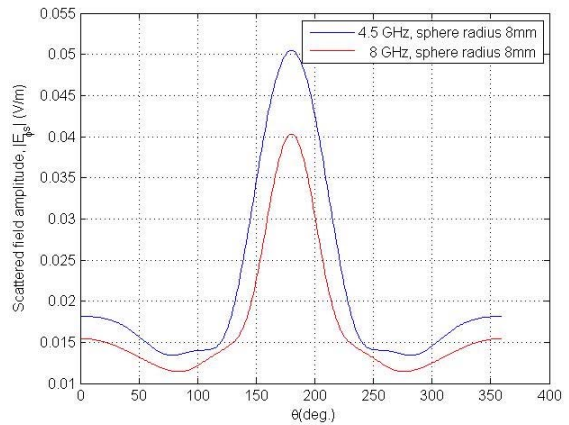


Figure 4. Comparison of scattered field, $|E_{\phi s}|$ with respect to observation angles, for different frequencies for a dielectric sphere radius of 8mm (incident angle is constant, 180°)

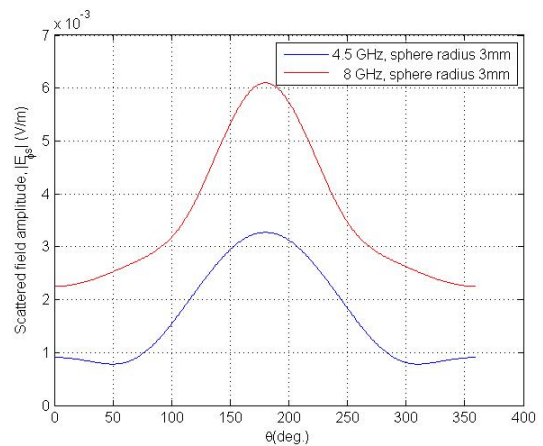


Figure 5. Comparison of scattered field, $|E_{\theta s}|$ with respect to observation angles, for different frequencies for a dielectric sphere radius of 3mm (incident angle is constant, 180°)

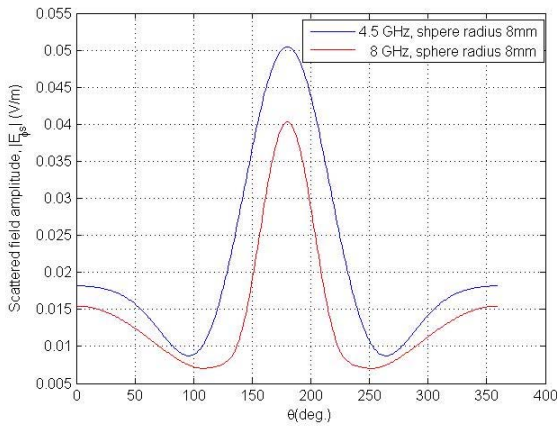


Figure 6. Comparison of scattered field, $|E_{\theta s}|$ with respect to observation angles, for different frequencies for a dielectric sphere radius of 8mm (incident angle is constant, 180°)

When the scattered fields of a dielectric sphere with 16 mm diameter inside different dielectric mediums are compared, it is observed that the scattered field is decreased inside the medium, which has higher permittivity and conductivity values, as shown Fig. 7.

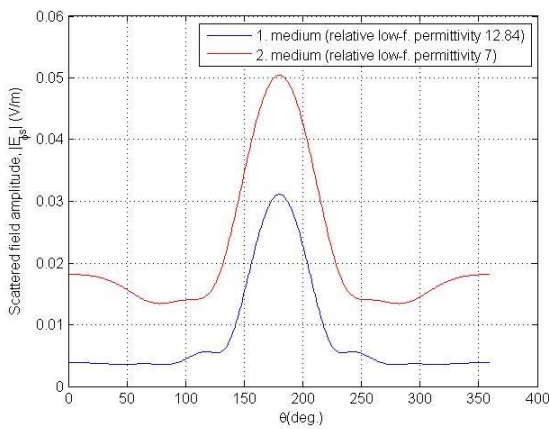


Figure 7. Comparison of scattered field by the dielectric sphere with 8 mm radius inside different dielectric mediums.

As shown in the Figure 8, the simulation is performed frequencies between 1 GHz and 8GHz in CST Microwave Studio. Measurements are done when there is nothing between the antennas. Graphic in the Figure 9 shows S11-parameter versus the frequency from 1 to 8GHz.

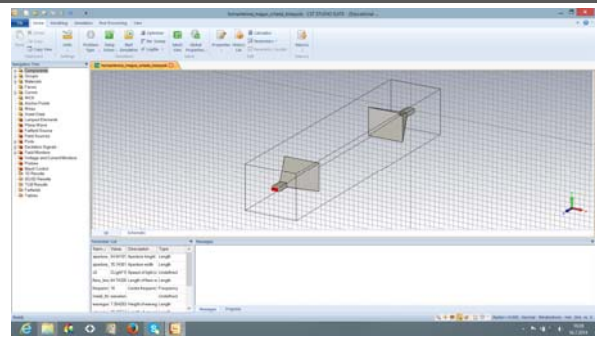


Figure 8. Measurement Setup of Simulation in CST Microwave Studio

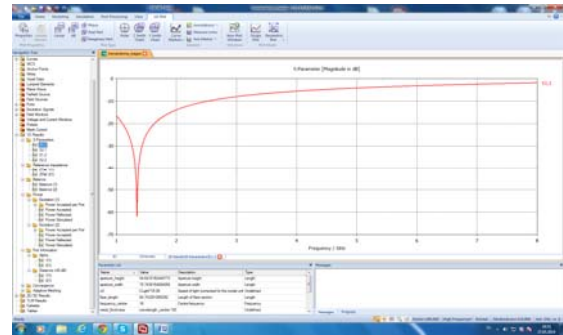
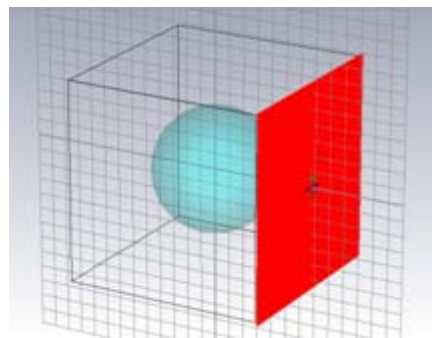


Figure 9. S11-parameter versus the frequency from 1 to 8GHz (there is nothing between the antennas)

As shown in the Figure 10, the simulation is performed when observation point is opposite the source. Measurements are done when there is a tumour model between the antennas. Graphic in the Figure 11 shows S11-parameter versus the frequency from 1 to 8GHz.



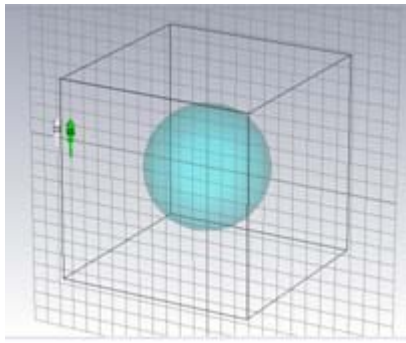


Figure 10. The illustration of the relationship of the source and observation point

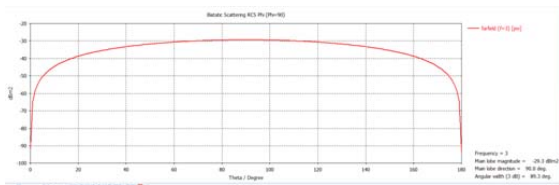


Figure 11. The result of the relationship of the source and observation point

As shown in the Figure 12, the simulation is performed when there is a breast model between the antennas. This breast model includes skin, fat, and fibro-glandular from outside to inside. Graphic in the Figure 13 shows Far-field of this simulation.

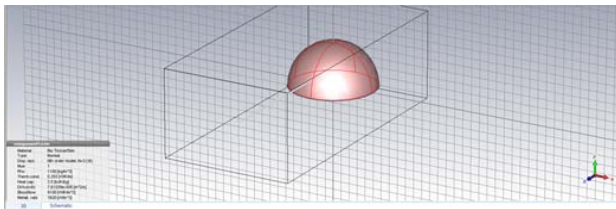


Figure 12. Simulation of the breast model in CST Microwave Studio

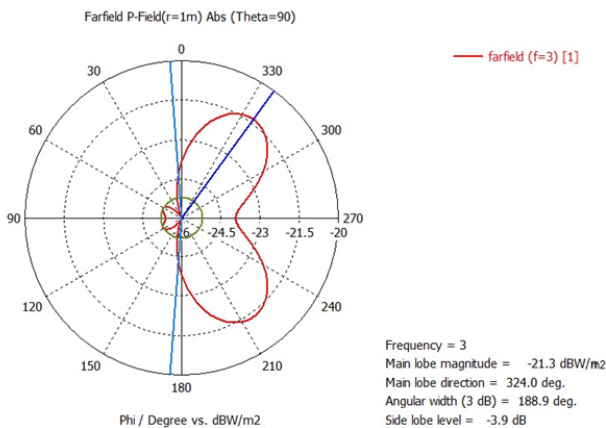


Figure 13. Simulation result of the breast model

As shown in the Figure 14, the simulation is performed when there is a breast model with tumour between the antennas. This breast model includes skin, fat, fibro-glandular, and tumour from outside to inside. Graphic in the Figure 14 shows Far-field of this simulation. It is seen that there is difference in simulation results between without tumours and with tumour.

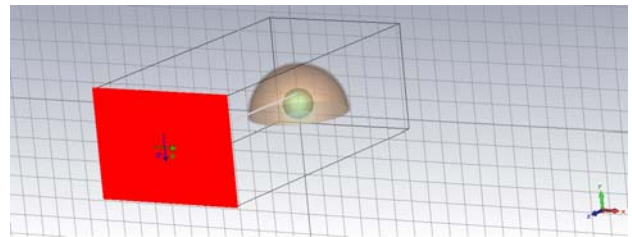


Figure 14. Simulation of the breast model with tumour in CST Microwave Studio

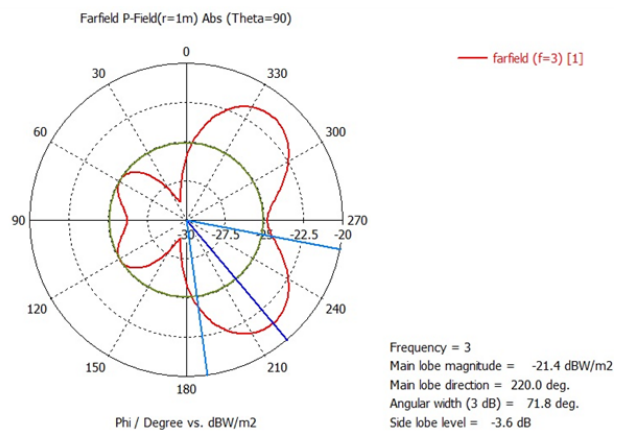


Figure 15. Simulation result of the breast model with tumour

In order to validate the accuracy of the analytical derivations, a full-wave electromagnetic solver CST Microwave Studio will be used for simulations in the future study.

4. Conclusion

An incident electromagnetic wave comes with different angles to sphere in the 1-8 GHz frequency range. Observation point is angular distance of pi from an incident wave. While an incident wave comes with a certain angle, observation point turns

from 0 to 360 degrees. According to this, scattered field amplitude is maximum at the location of incident wave, scattered field amplitude is minimum at the across incident wave. Graphic are shown for some incident angles and compared with the solution given by Harrington. Thus, the results are obtained faster and more reliable with reciprocal rotation. In addition, when there is another sphere with different properties in the outer sphere, the presence and location of the sphere will be detected faster. Therefore, it can be used in biomedical engineering as an alternative screening and diagnosis tool.

References

- STRUTT J., 1871. On the scattering of light by small particles. *Philosophical Magazine, series 4, vol. 41, p. 447.*
- LOVE, A. E. H., 1899. The Scattering of Electric Waves by a Dielectric Sphere. *Proceedings of the London Mathematical Society, Vol. 51-30, Issue 1, p. 308.*
- WESTON , V. H., and HEMENGER, R., 1962. High-Frequency Scattering From a Coated Sphere. *JOURNAL OF RESEARCH of the National Bureau of Standards- D. Radio Propagation Vol. 66D, No. 5, p. 613.*
- SWARNER, W. G. and PETERS, L., 1963. Radar Cross Sections of Dielectric or Plasma Coated Conducting Spheres and Circular Cylinders. *IEEE Transactions on Antenna and Propagation, p.558.*
- RHEINSTEIN, J., 1963. Scattering of Electromagnetic Waves from Dielectric Coated Conducting Spheres. *IEEE Transactions on Antenna and Propagation, p.334.*
- INADA H., PLONUS, M. A., 1970. The Diffracted Field Contribution to the Scattering from a Large Dense Dielectric Sphere. *IEEE Transactions on Antenna and Propagation, Vol. AP-18, No. 5, p.649.*
- RICHMOND, J. H., 1987. Scattering by a Ferrite-Coated Conducting Sphere. *IEEE Transactions on Antenna and Propagation, Vol. AP-35, No. 1, p.73.*
- HILL, D. A., 1988. Electromagnetic Scattering by Buried Objects of Low Contrast. *IEEE Transactions on Geoscience and Remote Sensing, Vol. 26, No. 2, p.195.*
- HAMID, A. K., CIRIC, I. R., and HAMID M., 1991. Iterative Solution of the Scattering by an Arbitrary Configuration of Conducting Of Dielectric Spheres. *IEE Proceedings-H, Vol. 138(6), p. 565.*
- GENG Y., L., QIU C. W., and YUAN, N., 2009. Exact Solution to Electromagnetic Scattering by an Impedance Sphere Coated With a Uniaxial Anisotropic Layer. *IEEE Transactions on Antennas and Propagation, Vol. 57, No. 2, p. 572.*
- HARRINGTON, R. F., 1961. Time-Harmonic Electromagnetic Fields. *The United States of America, 480p.*
- KIM, T. H., and PACK, J. K., 2012. Measuremet of Electrical Characteristics of Female Breast Tissues for the Development of the Breast Cancer Detection. *Progress In Electromagnetics Research C, Vol. 30, 189-199.*
- KORENEV, B. G., 2002. Bessel Functions and Their Applications. *The Unites States of America, CRC Press LLC.*
- MALICKY, P., and MALICKA, M., 1990. On the computation of Riccati Bessel functions. *Aplikace matematiky, Vol. 35, No. 6, 487-493.*
- MARGERUM, E. A., and VAND, V., 1964. Light Scattering By Small Graphite Spheres. *Monthly Notices of the Royal Astronomical Society, Vol. 128, p. 431.*